Quasiparticle electronic structure of barium-silicon oxynitrides for white-LED application

B. Bertrand,[1,2,*] S. Poncé,[1,*] D. Waroquiers,[1] M. Stankovski,[1] M. Giantomassi,[1] M. Mikami,[3] and X. Gonze[1]

[1]*European Theoretical Spectroscopy Facility, Institute of Condensed Matter and Nanosciences, Université catholique de Louvain, Chemin des étoiles 8, bte L07.03.01, B-1348 Louvain-la-neuve, Belgium*

[2]*CERDECAM, Institut Supérieur Industriel ECAM, Promenade de l'Alma 50, B-1200 Bruxelles, Belgium*

[3]*Mitsubishi Chemical Group, Science and Technology Research Center, Inc., 1000, Kamoshida-cho Aoba-ku, Yokohama, 227-8502, Japan*

$Ba_3Si_6O_{12}N_2$:Eu^{2+} and $Ba_3Si_6O_9N_4$:Eu^{2+} have strikingly similar atomistic structures, but the former is an efficient green phosphor at working temperature while the latter is a bluish-green phosphor whose luminescence decreases quite fast with temperature. Aiming at the understanding of such different behavior, we compute the quasiparticle electronic band structure of the two hosts, $Ba_3Si_6O_{12}N_2$ and $Ba_3Si_6O_9N_4$, thanks to many-body perturbation theory in the G_0W_0 approximation. The gap differs by about 0.43 eV. We analyze the eigenfunctions at the top of the valence band, at the bottom of the conduction band, and also the chemical shifts for the Ba site in the two hosts. The valence bands, directly impacted by the different stoichiometric ratio, are not thought to play a large role in the luminescence. Deceivingly, the dispersive bottom of the conduction band, directly related to luminescent properties, is similar in both compounds. The spatial topology of the probability density of the bottom of the conduction bands differs, as well as the location of the 5d peak, with a much higher energy than the bottom of the conduction band in $Ba_3Si_6O_{12}N_2$ than in $Ba_3Si_6O_9N_4$. Electromagnetic absorption spectra are also computed for both compounds.

PACS number(s): 71.20.Ps, 78.20.−e, 42.70.−a

I. INTRODUCTION

After the recent invasion of compact fluorescent lamps, white LED lighting is becoming a major contender in ecofriendly light sources, with a combination of green- and red-emitting phosphors partly absorbing the blue light emitted by an InGaN LED.[1,2] Phosphors with optimized luminescence properties (i.e., with an optical spectrum close to the solar one and low thermal quenching) are coveted by industry and the subject of very active development. A detailed theoretical understanding of their electronic structure is still lacking and might aid experimental researchers in finding more efficient phosphors.

In this spirit, we have studied two chemically close oxynitride materials, in which rare-earth europium doping lead to different luminescence properties. The recently discovered green phosphor $Ba_3Si_6O_{12}N_2$:Eu^{2+} offers very good luminescence properties and weak thermal quenching[3,4] at working temperature (around 100 °C), while $Ba_3Si_6O_9N_4$:Eu^{2+} is a bluish-green phosphor that exhibits an unfavorable decrease of the luminescence intensity with temperature.[3–5] The crystal structure of $Ba_3Si_6O_9N_4$:Eu^{2+} was reported by Stadler *et al*.[6] The original result of Uheda *et al*.[3] for $Ba_3Si_6O_{12}N_2$:Eu^{2+} was confirmed and studied in more depth by further experimental studies.[5,7–12] In particular, Braun *et al*.[8] evaluated the $Ba_3Si_6O_{12}N_2$ band gap to be 7.05 eV by means of x-ray emission spectroscopy (XES) and x-ray absorption near edge spectroscopy (XANES).

The crystalline structure of these two materials is very similar: Si-O-N layers alternate with Ba layers, while the Si-O-N layers are made of tetrahedra with silicon at their center, and O or N at their apices, connected through Si-O-Si or Si-N-Si bonds. The lattice parameters are similar as well. The Ba environment is more subject to variations, not only in the two materials, but also for different crystalline positions within one material: Although predominantly made of O atoms, some

Ba are not close to any N atom, while some have one, two, or three N neighbors. The Eu dopant might substitute any of these sites. With such apparently similar materials, one can wonder why the quenching temperature is so different. In particular, this might indicate the extent to which a search for good luminescent materials has to take into account small details of the crystalline structure of the host.

Despite their similar structure and chemical formula, the different optical characteristics as a function of temperature might enable one to single out basic factors influencing their fluorescence properties. Empirical hypotheses have been brought up by Mikami *et al*.[4] They postulated that $Ba_3Si_6O_9N_4$:Eu^{2+} experienced a stronger thermal quenching because the lowest Eu-d states are closer to the conduction bands than in the $Ba_3Si_6O_{12}N_2$:Eu^{2+} case. The photoexcited 5d electrons of Eu^{2+} would then be thermally ionized to the conduction bands at room temperature following the Dorenbos model[13] (autoionization). In general, it is difficult to experimentally determine band gaps of phosphors, because phosphor samples are usually obtained as powder, so this assertion can only be verified through comprehensive numerical analysis with sufficient accuracy, on the order of a few sub-eV for the thermal quenching temperature.[14]

The hosts and doped materials have been studied from the *ab initio* point of view as well. Mikami *et al*.[4] obtained an electronic band gap of 4.63 eV and 4.37 eV (resp.) for $Ba_3Si_6O_{12}N_2$ and $Ba_3Si_6O_9N_4$ (resp.). They used generalized-gradient approximation (GGA) within the density functional theory (DFT).[15,16] Such an approach is subject to the well-known DFT *band gap problem*: The gap is usually underestimated, sometimes strongly. Braun *et al*.[8] found an indirect band gap (A-Γ) of 4.8 eV for $Ba_3Si_6O_{12}N_2$ using GGA and went further by also using a modified Becke-Johnson potential (mBJ-GGA), known to give a much better global agreement with true gap values, albeit for the wrong reasons,[17]

leading to a value of 6.93 eV. Tang *et al.*[9] performed DFT + U calculations for the Eu-doped compounds using a supercell ($Ba_{11}Si_{24}O_{48}N_8Eu$). They obtained a direct gap of 1.3 eV between the Europium 4f states and the excited 5d state of barium. Still, the accuracy of DFT + U computation for such a 4f-5d gap is also questionable.

Unlike previous DFT-based studies, we compute the band structure of these materials by state-of-the-art many-body perturbation theory in the so-called G_0W_0 approximation,[18] which is much more computationally demanding than DFT, but reliably gives band gaps within 10% of the experimental value, usually underestimating it.[19] To our knowledge, it has not yet been used for LED phosphors (neither Eu-based ones nor Ce-based ones). Our G_0W_0 band gap is indeed very close to the experimental band gap for $Ba_3Si_6O_{12}N_2$. The narrowing of the gap between $Ba_3Si_6O_{12}N_2$ and $Ba_3Si_6O_9N_4$ is confirmed. We then perform different analyses to characterize the differences in electronic structure and optical properties in both compounds, and find that the opening of the gap is more related to valence band modifications than to conduction band ones, while the reverse would be expected in order to establish the link to different luminescent behavior. Thus, calculations on doped hosts are needed to clarify the situation. The fact that such detailed calculation might be needed is somehow problematic, in view of rapid first-principle screening of materials in large databases, which is an emerging technique to explore the huge variety of materials.[20]

After the present introduction, we detail our numerical approach. In Sec. III, we analyze successively the crystallographic structure, the quasiparticle band structure and density of states, the effective masses, and then discuss energy shifts, electrostatic potential, and absorption spectra in both materials, before concluding.

II. NUMERICAL APPROACH

We have used projector augmented wave (PAW)[21] pseudopotentials with the Perdew-Burke-Ernzerhof parametrization of the generalized gradient approximation[22] for the exchange-correlation functional. Due to the precise nature of the PAW numerical method, which includes information about rapidly varying wave functions in atomic core regions, the quality of the results should be very close to that of all-electron calculations, despite the fact that the PAW methodology assumes a selected set of core electrons to be frozen and a finite number of projectors on valence states (or semicore states) replacing a formally infinite one, as detailed below. Crucially, we have found that a reliable computation of the G_0W_0 corrections to the LDA band gap requires the explicit treatment and relaxation of semicore states in the PAW atomic data for barium.

We have generated a PAW atomic data set for barium taking the $4d^{10}5s^25p^66s^2$ orbitals as valence states, and considering the states below as frozen. The PAW sphere radius is 2.45 Bohr with three projectors per occupied angular momentum channel. A large number of projectors is sometimes required for perturbative calculations, where the unoccupied states are used as a basis and therefore need to be accurately described. Increasing the number of projectors improves the flexibility of the basis and hence allows for an accurate reproduction of the all-electron wave function. We have used the software

ATOMPAW[23] to generate the barium PAW pseudopotential. The other PAW pseudopotentials were taken from the ABINIT website.[24] The silicon PAW data set with $3s^23p^2$ valence electrons has a 1.71 Bohr sphere radius and two projectors per angular momentum channel. Oxygen with $2s^22p^4$ valence electrons has a 1.2 Bohr sphere radius and three projectors per angular momentum channel. The nitrogen with $2s^22p^3$ valence electrons has a 1.3 Bohr radius and two projectors per angular channel. With these pseudopotentials we made a structural relaxation of the cell geometry and atoms positions using a Broyden-Fletcher-Goldfarb-Shanno (BFGS) minimization scheme[25] at the DFT level.

While DFT approaches usually underestimate the band gap, many-body perturbation theory is a well established technique that delivers an accurate quasiparticle band structure. We rely on Hedin's GW approximation, applied perturbatively (so-called G_0W_0 corrections): From the DFT wave functions and eigenenergies we computed the screening of the system in the random phase approximation and extract the quasiparticle correction to the band gap by computing the G_0W_0 self-energy correction.[26]

We computed the quasiparticle correction on a $6 \times 6 \times 4$ Monkhorst-Pack sampling[27] of the Brillouin zone half-shifted along the z direction. The quasiparticle band structure was then obtained using an energy-dependent polynomial fit of the G_0W_0 eigenenergies.[17] This approach is significantly better than the cruder usual method of using a constant scissor shift for all unoccupied bands, and leads to similar results as provided by a Wannier interpolation[28] but is easier to use and less computationally demanding. A cutoff energy of 25 Ha was used for the plane-wave basis set to describe the wave functions, and a converged cutoff energy of 6 Ha was chosen for the plane-wave set representing the independent-particle susceptibility and the dielectric matrix for the calculation of the screening.

A number of efficient approaches to the calculation of the GW self-energy have recently been developed such that only a small number of unoccupied states are required for the perturbation expansion summation. Among them, the *extrapolar method*[29] consists of introducing an average pole energy to replace the poles arising from the eigenvalues of empty states beyond an arbitrary energy level. This allows for the truncation of the sum over states in the screening or self-energy calculation and improves convergence with respect to the number of unoccupied bands, while keeping unmodified the final converged value. We have chosen an extrapolar energy of 2.5 Ha for the screening calculation (and 2 Ha for the self-energy). This reduces by a factor of five the number of empty states required for a convergence of the gap to within 0.01 eV for both screening and self-energy calculations. In both cases, 340 unoccupied bands were explicitly treated in the sums.

We have used a Godby-Needs[30] plasmon-pole model to evaluate the self-energy operator $\Sigma(\omega)$. A computationally more demanding fully frequency-dependent numerical integration by the contour deformation (CD) technique[31] was also undertaken to assess the quality of the plasmon-pole model. The CD calculation was made only at the Γ point for $Ba_3Si_6O_{12}N_2$ and reveals a discrepancy of the band gap of less than 0.4% with respect to the plasmon-pole model approach.

We have consequently chosen to make all further calculation with this plasmon-pole model. After a careful convergence analysis, the estimated numerical error (within the chosen approximations, as explained above) is about 0.1 eV.

We also have computed the electromagnetic (optical + UV) absorption spectra [imaginary part of the macroscopic dielectric function $\varepsilon(\omega)$] of the two materials in the independent particle sum over states approximation, also called random phase approximation (RPA).[32] The relative convergence below 1% of the absorption spectrum in the energy range considered required a $6 \times 6 \times 6$ k-point grid. The convergence on the number of bands included in the calculations is crucial for RPA calculation. The transition between the 38 highest valence bands and the 67 lowest conduction bands were taken explicitly into account for the case of $Ba_3Si_6O_{12}N_2$. For $Ba_3Si_6O_9N_4$ the 44 highest valence bands and the 71 lowest conduction bands were needed. We used a scissor of 2.258 eV for $Ba_3Si_6O_{12}N_2$ and 2.07 eV for $Ba_3Si_6O_9N_4$ to account for the opening of the quasiparticle band gap between DFT and GW. All calculations have been done using the ABINIT software.[33]

III. RESULTS AND DISCUSSION

A. Crystallographic structure

The space group of $Ba_3Si_6O_{12}N_2$ is found to be $P\bar{3}$ (trigonal, 147). DFT structural relaxation leads to lattice constants $a = 7.608$ Å and $c = 6.553$ Å. This theoretical result is slightly above the experimental values given by Braun et al.[8] of 7.5218(1) Å and 6.4684(1) Å, although well within the expectations of GGA functionals, which tend to overestimate slightly the bond lengths.

As shown in Fig. 1, $Ba_3Si_6O_{12}N_2$ is built up of corner-sharing SiO_3N tetrahedra forming corrugated layers between which the Ba^{2+} ions are located.[4] The latter ions occupy two different crystallographic sites: (i) One barium atom denoted by Ba_1 occupies Wyckoff position 1a and is surrounded by six symmetrically equivalent oxygen atoms forming a trigonal antiprism (distorted octahedron). (ii) Two barium atoms denoted by Ba_2 occupy Wyckoff positions 2d and are surrounded by six oxygen atoms forming a trigonal antiprism, further capped with a nitrogen atom.

As described by Stadler et al.[6] the Ba^{2+} ions occupy three different crystallographic sites in the crystal structure of $Ba_3Si_6O_9N_4$. In the latter reference, it is mentioned that two of them are trigonal antiprisms with six oxygen atoms (Ba_1 and Ba_3) while the other is a trigonal antiprism with six oxygen atoms, further capped with a nitrogen atom (Ba_2). However, a look at neighbors in a slightly larger environment reveals that Ba_1 is also close to three nitrogen atoms forming a triangle perpendicular to the z axis, while there exists another nitrogen atom close to the Ba_2, opposite to the first one, along the z direction, as shown in Fig. 2. The DFT structural relaxation for this second host gives two lattice constants of $a = 7.323$ Å and $c = 6.863$ Å also somewhat larger than the experimental value by Stadler et al.[6] of 7.249(1) Å and 6.784(5) Å. The crystallographic figures are made using the VESTA software.[34]

The selected bond lengths and bond angles of the two host materials are shown in Table I and compared with experiment and previous GGA calculations using NC pseudopotentials.
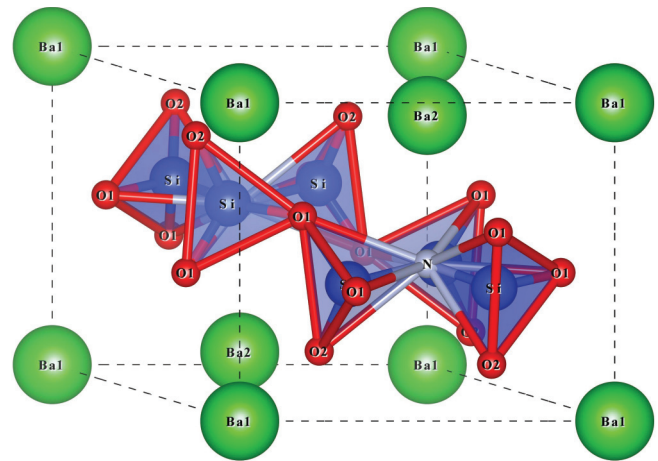
(a) $Ba_3Si_6O_{12}N_2$
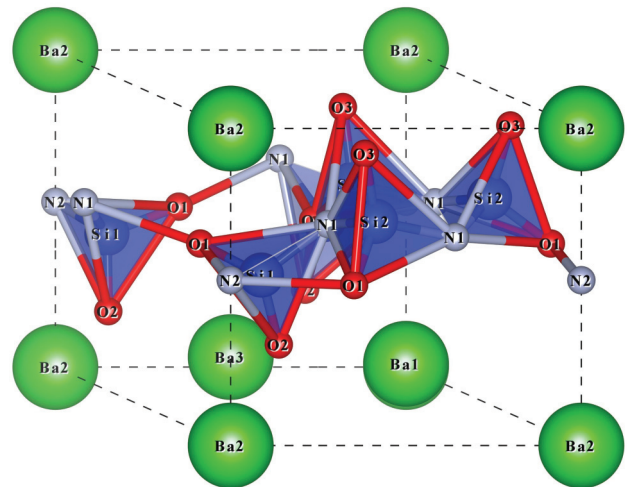
(b) $Ba_3Si_6O_9N_4$

FIG. 1. (Color online) (a) Crystal structure of $Ba_3Si_6O_{12}N_2$ after structural relaxation. There are two inequivalent barium atoms. The first one is labeled Ba_1 and occupies the 1a Wyckoff position and the other labeled Ba_2 is in the 2d Wyckoff position. Figure (b) shows the crystal structure of $Ba_3Si_6O_9N_4$ after structural relaxation. There are three inequivalent barium atoms. The first one is labeled Ba_1 and occupies the 1c Wyckoff position, the second one labeled Ba_2 is in the 1a Wyckoff position, and the last one named Ba_3 is in the 1b Wyckoff position.

The O-(O,N)-O angles of $Ba_3Si_6O_{12}N_2$ range from 135–161° and correspond well with experimental data from Braun et al.[8] that range from 135–160°. The Si-N-Si angles of $Ba_3Si_6O_9N_4$ range from 117–121° and also matches the experimental results of Stadler et al.[6] that range from 116–121°.

B. Quasiparticle band structure and density of states

The computed quasiparticle electronic band structure based on the one-shot G_0W_0 approximation with PAW pseudopotentials is given in Fig. 3. $Ba_3Si_6O_{12}N_2$, with theoretical structure, has an indirect Γ-A fundamental gap of 6.88 eV, slightly underestimating the experimental gap value of 7.05 ± 0.25 eV.[8] Such slight underestimation is often observed from

(a) Ba$_1$ in Ba$_3$Si$_6$O$_{12}$N$_2$

(b) Ba$_2$ in Ba$_3$Si$_6$O$_{12}$N$_2$

(c) Ba$_1$ in Ba$_3$Si$_6$O$_9$N$_4$

(d) Ba$_2$ in Ba$_3$Si$_6$O$_9$N$_4$
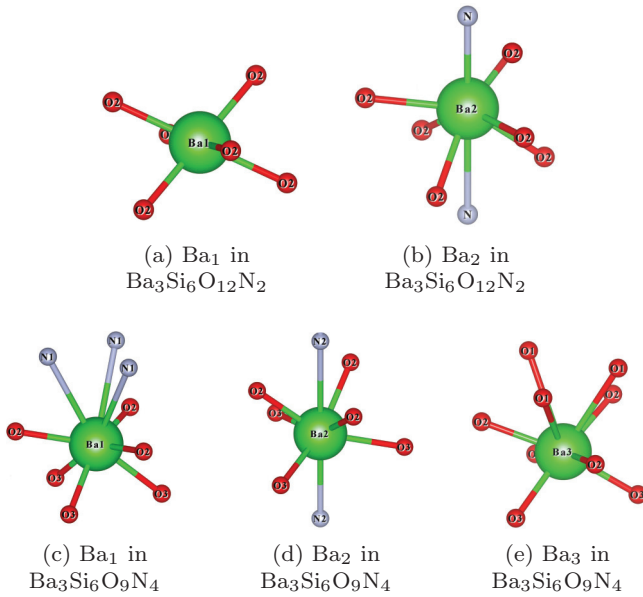
(e) Ba$_3$ in Ba$_3$Si$_6$O$_9$N$_4$

FIG. 2. (Color online) (a) and (b) show the crystalline environment of the two inequivalent barium atoms in Ba$_3$Si$_6$O$_{12}$N$_2$. (c)–(e) show the crystalline environment of the three inequivalent barium atoms in Ba$_3$Si$_6$O$_9$N$_4$. Bond lengths are reported in Table I.

TABLE I. Selected bond lengths [in Å] of Ba$_3$Si$_6$O$_{12}$N$_2$ and Ba$_3$Si$_6$O$_9$N$_4$ compounds.

	Ba$_3$Si$_6$O$_{12}$N$_2$		
	GGA-PAW	GGA-NC[a]	Experimental[b]
Ba$_1$-O$_2$ (6x)	2.7596	2.774	2.744(3)
Ba$_2$-O$_2$ (3x)	2.9590	2.960	2.902(3)
-O$_2$ (3x)	2.8121	2.834	2.819(3)
-N (1x)	3.054	3.041	2.997(6)
-N (1x)	3.499	3.261	3.471(6)
Si-N (1x)	1.7550	1.750	1.735(2)
-O$_1$ (1x)	1.6716	1.663	1.649(3)
-O$_1$ (1x)	1.6741	1.664	1.650(4)
-O$_2$ (1x)	1.6127	1.600	1.587(3)
	Ba$_3$Si$_6$O$_9$N$_4$		
Ba$_1$-O$_2$ (3x)	2.714	2.731	2.688(4)
-O$_3$ (3x)	2.823	2.836	2.824(4)
-N$_1$ (3x)	3.498	3.480	3.413(5)
Ba$_2$-O$_2$ (3x)	2.703	2.727	2.704(4)
-O$_3$ (3x)	2.860	2.868	2.833(4)
-N$_2$ (1x)	3.284	3.232	3.156(7)
-N$_2$ (1x)	3.579	3.648	3.627(7)
Ba$_3$-O$_2$ (3x)	2.730	2.741	2.710(4)
-O$_3$ (3x)	2.731	2.756	2.724(4)
-O$_1$ (3x)	3.375	3.381	3.133(4)
Si$_1$-O$_2$ (1x)	1.628	1.615	1.605(4)
-O$_1$ (1x)	1.672	1.663	1.644(5)
-N$_1$ (1x)	1.751	1.746	1.734(5)
-N$_2$ (1x)	1.764	1.759	1.746(2)
Si$_2$-O$_3$ (1x)	1.623	1.610	1.595(4)
-O$_1$ (1x)	1.674	1.666	1.649(4)
-N$_1$ (1x)	1.756	1.750	1.738(5)
-N$_1$ (1x)	1.772	1.767	1.754(5)

[a]See Ref. 4 for Ba$_3$Si$_6$O$_{12}$N$_2$ and Ba$_3$Si$_6$O$_9$N$_4$.
[b]See Ref. 8 for Ba$_3$Si$_6$O$_{12}$N$_2$ and Ref. 6 for Ba$_3$Si$_6$O$_9$N$_4$.

G_0W_0 methods.[19] This is in even better agreement whenever the G_0W_0 calculation is applied to Ba$_3$Si$_6$O$_{12}$N$_2$ with the experimental structure, for which the obtained band gap is 7.00 eV. Ba$_3$Si$_6$O$_9$N$_4$ has an indirect Γ-M band gap of 6.45 eV at the theoretical structure.

The fundamental gap of Ba$_3$Si$_6$O$_9$N$_4$ is thus 0.43 eV smaller than the one of Ba$_3$Si$_6$O$_{12}$N$_2$. This is in agreement with the phenomenological interpretation of the quenching mechanism according to the Dorenbos's scheme.[13,35] We will now discuss the narrowing of the gap in terms of factors related to valence band differences and conduction band differences. Note, however, that we did not attempt to compute accurate band offsets between the two hosts, as an accurate prediction would need larger supercells.

The density of states, and the partial density of states for the Ba$_d$, Ba$_s$, O$_p$, and N$_p$ states is also presented in Fig. 3. The top of the valence bands is dominated by the N$_p$ states in both compounds. Two bands clearly emerge from the block of valence bands in Ba$_3$Si$_6$O$_{12}$N$_2$, while four bands emerge for Ba$_3$Si$_6$O$_9$N$_4$. These numbers of bands can be correlated with the existence of nonbonding N$_p$ states, one for each nitrogen atom. The apparition of the two extra valence nitrogen states in Ba$_3$Si$_6$O$_9$N$_4$ pushes the two other nitrogen states higher in energy. This is clearly a factor leading to the lowering of the band gap.

The analysis of the conduction band complex is particularly relevant as well, as in both cases one strongly dispersive band is observed, coming from a combination of Ba$_s$ and O$_p$ states. The electrons excited in this conduction band will have a rather high mobility, and thus might approach a luminescence killer defect, regardless of its origin. We will analyze these orbitals, and associated effective mass later. Above the strongly dispersive band, a large set of flatter bands is observed, 8.63 eV higher than the valence band maximum in the case of Ba$_3$Si$_6$O$_{12}$N$_2$,

and 7.70 eV higher in the case of Ba$_3$Si$_6$O$_9$N$_4$. They arise mainly from the Ba$_d$ channel, albeit mixed with other orbitals. The large difference between the two hosts for the dominant peak in the conduction DOS will have to be investigated.

Before performing this analysis, and in line with the PDOS analysis, we present the G_0W_0 corrections to the DFT eigenenergies for the two hosts, shows in Fig. 4. The relatively large range of corrections (up to 0.5 eV spread) for the excited states between 6 and 7 eV (DFT energy, giving G_0W_0 energy between 10 and 11 eV above the valence band maximum) is to be related to the strong hybridization between the 5d and 6s levels of barium. On the other hand the narrow dispersion of corrections below 6 eV is related to the well defined 6s states of barium. This illustrates the validity of our interpolation scheme for the valence bands and the lowest conduction band, but also its limit for the higher bands.

C. Effective masses

The effective mass at a given k-point k and band index n is defined as

$$m_{nk}^* = \hbar^2 \left(\frac{\partial^2 \varepsilon_{nk}}{\partial k^2} \right)^{-1},$$
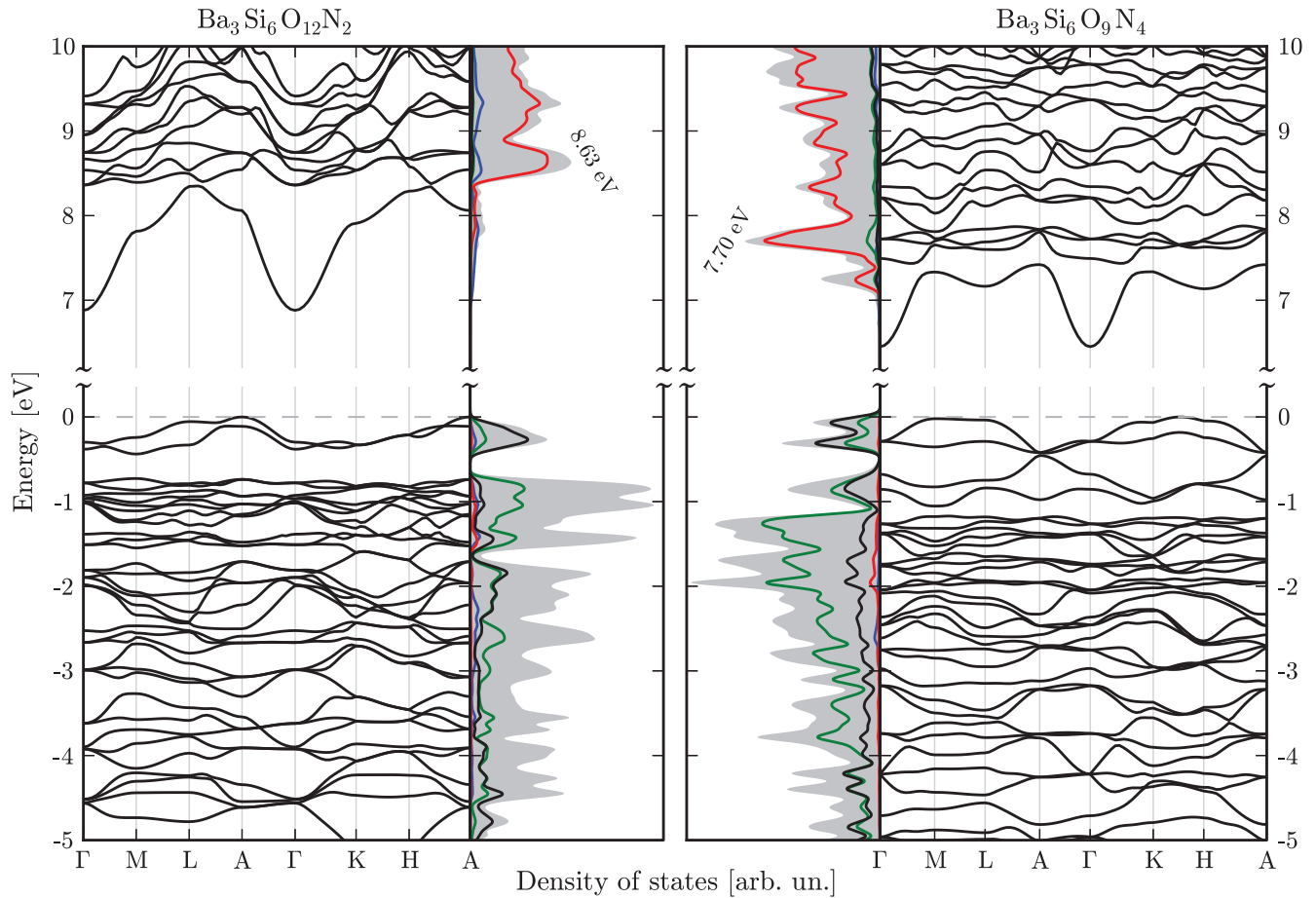
FIG. 3. (Color online) On the left side: the G_0W_0 Ba$_3$Si$_6$O$_{12}$N$_2$ quasiparticle band structure and on the right side: the G_0W_0 Ba$_3$Si$_6$O$_9$N$_4$ quasiparticle band structure. The red line is the partial density of state (PDOS) of the Ba$_d$ level, the blue line is the PDOS of the Ba$_s$ level, the green line is the PDOS of the O$_p$ level, and the black line is the PDOS of the N$_p$ level. The gray area is the total density of states (DOS).

with ε_{nk} the eigenenergy at a given k point k and band index n. The effective masses of the electrons at the bottom of the conduction band in the direction Γ-A and Γ-K are 0.481 and 0.503 for Ba$_3$Si$_6$O$_{12}$N$_2$ in DFT, respectively. For
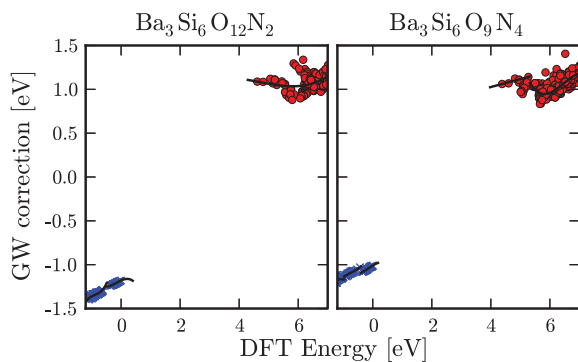
FIG. 4. (Color online) Magnitude of G_0W_0 corrections to the DFT eigenenergies for Ba$_3$Si$_6$O$_{12}$N$_2$ on the left side and Ba$_3$Si$_6$O$_9$N$_4$ on the right side. The negative corrections (blue crosses) are for the occupied states and the positive (red dots) for the unoccupied states. The full line shows the energy polyfit that was used to generate the quasiparticle band structure in Fig. 3.

Ba$_3$Si$_6$O$_9$N$_4$ in the direction Γ-A and Γ-K we have 0.446 and 0.491 at the DFT level, respectively (effective masses from the polyfit interpolation scheme do not include k-dependent corrections,[36] and it is preferable to stick to the DFT values). The effective masses are smaller in the direction Γ-A. In Fig. 5, the square of the wave function at the bottom of the conduction band is presented. For Ba$_3$Si$_6$O$_{12}$N$_2$, one sees that in this direction (along the z axis and perpendicular to the barium plane) the density creates a channel linking the Ba$_1$. Another view from the top in Fig. 6 shows that in Ba$_3$Si$_6$O$_{12}$N$_2$ the density has a sixfold symmetry that point towards the six silicon atoms (three are in the upper plane and three are in the down plane). The states in that direction will be more delocalized and hence the energy dispersion will be steeper, with a smaller effective mass in that direction. Opposite to one may think it is not the Ba$_2$ close to the nitrogen that conduct the electrons of the unoccupied band but the Ba$_1$.

The main difference between the two compounds, for the conduction band, thus lies in the fact that the barium atom that has the biggest weight in the first unoccupied state is the one surrounded only by oxygen in the case of Ba$_3$Si$_6$O$_{12}$N$_2$ (Ba$_1$) and the one close to three nitrogen in the case of Ba$_3$Si$_6$O$_9$N$_4$ (Ba$_1$).
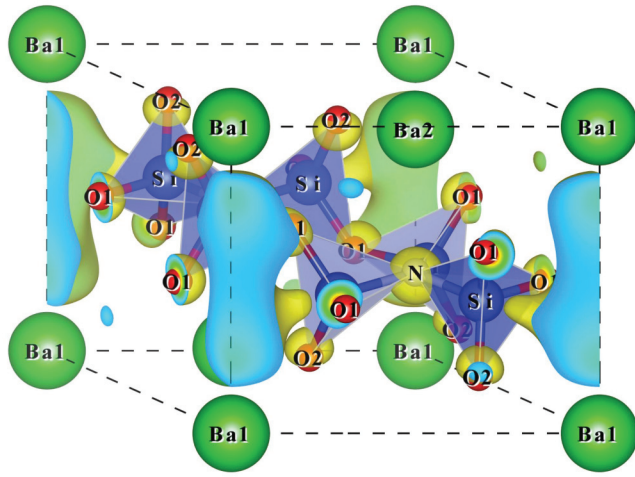
(a) $Ba_3Si_6O_{12}N_2$
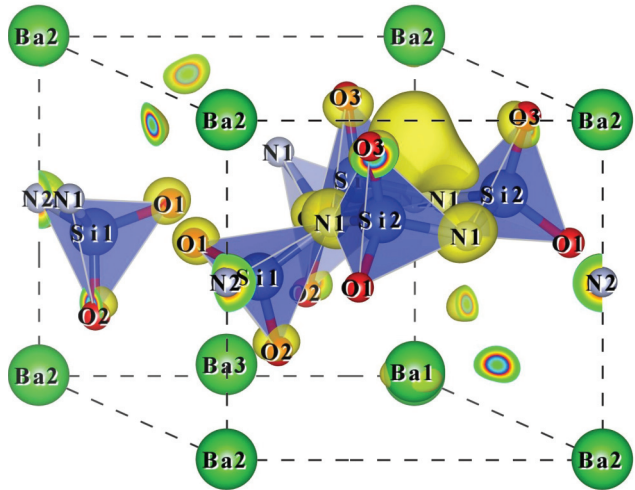
(b) $Ba_3Si_6O_9N_4$

FIG. 5. (Color online) (a) Density of the first unoccupied band (84th band) of $Ba_3Si_6O_{12}N_2$ at the Γ point, that is $\Psi^*_{84\Gamma}\Psi_{84\Gamma}$. The channel density corresponds mainly to the 6s state of barium. (b) Density of the first unoccupied band (80th band) of $Ba_3Si_6O_9N_4$ at the Γ point, that is $\Psi^*_{80\Gamma}\Psi_{80\Gamma}$. Both isodensity are at 10% of the maximum density of that state. Large values are located around nitrogen and oxygen atoms.

D. Energy shifts and electrostatic potential

We now turn to the analysis of the DOS peaks, attributed to Ba_{5d} states. The fact that the 5d states are 0.93 eV lower in energy in $Ba_3Si_6O_9N_4$ (7.70 eV) than in $Ba_3Si_6O_{12}N_2$ (8.63 eV), and closer to the conduction band minimum, might be important to explain the thermal quenching. Indeed, in the europium-doped material, the europium is substitutional to some of the barium atoms. If the local electrostatic potential at the barium site is lower in one (or another) site of one of the host materials, it should also be lower when the europium has replaced the barium. Obviously, a further shift due to the substitution might be present as well, but is expected to be similar in the two materials. Also, the lowering of the 5d states might not be due to the electrostatic potentials, but to different hybridization with orbitals from neighboring atoms.
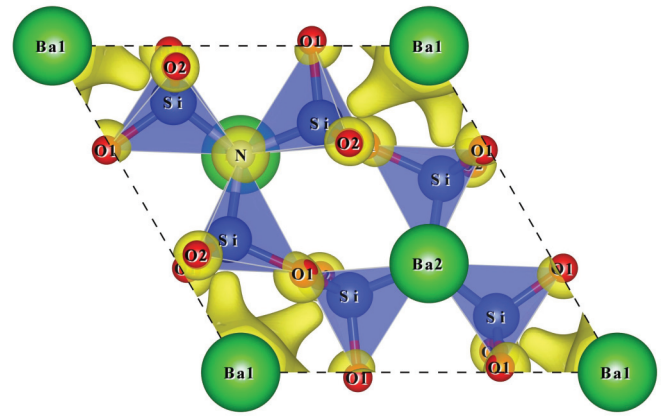
(a) $Ba_3Si_6O_{12}N_2$
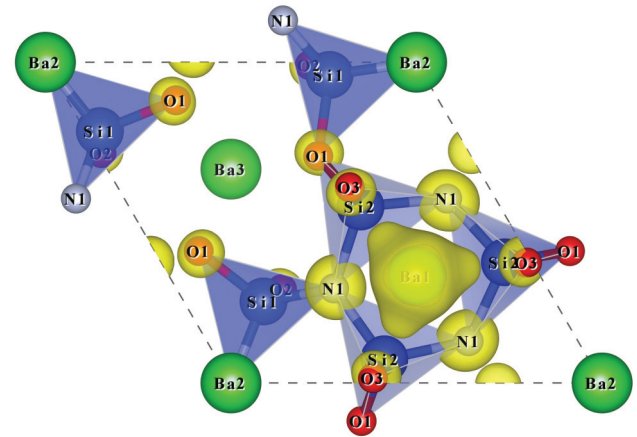
(b) $Ba_3Si_6O_9N_4$

FIG. 6. (Color online) (a) Density of the first unoccupied band (84th band) of $Ba_3Si_6O_{12}N_2$ at the Γ point seen from the top. (b) Density of the first unoccupied band (80th band) of $Ba_3Si_6O_9N_4$ at the Γ point seen from the top. Both isodensity are at 10% of the maximum density of that state.

In order to analyze the local electrostatic potential and in addition to the analysis performed at the vicinity of the band gap, we have gathered information on the electronic structure for a larger range of energies in Table II, including band edges, bandwidths, and the dominant band characters for both hosts.

Directly influenced by the local electrostatic potential at the atomic site, the 4d core levels of barium are located lower in energy in $Ba_3Si_6O_9N_4$ than in $Ba_3Si_6O_{12}N_2$, with respect to the top of the valence band. However, the difference is not very large (about 0.2 eV). We note that the local electrostatic potential is not the same in the different locations for each host. The Ba_{4d} levels at the Ba_2 site in $Ba_3Si_6O_{12}N_2$ are about 0.3 eV lower than the Ba_{4d} level at the Ba_1 site. Similarly the Ba_{4d} levels at the Ba_1 and Ba_2 sites are about 0.26 eV lower than at the Ba_3 site for $Ba_3Si_6O_9N_4$. The spread of the Ba_{5s} bands, combining contributions from the three sites, is on the order of 0.27 eV, for both hosts, with a chemical shift between the two hosts that is similar to the one of the Ba_{4d} states. From this analysis, the local electrostatic potential only explains a fraction of the 0.93 eV shift of the 5d states.

TABLE II. Band positions [eV], bandwidth [eV], and the dominant band character of $Ba_3Si_6O_{12}N_2$ and $Ba_3Si_6O_9N_4$ compounds. The number in parenthesis for the bandwidth is the number of bands in that group.

Position DFT	Bandwidth DFT	Position G_0W_0	Bandwidth G_0W_0	Band character
		$Ba_3Si_6O_{12}N_2$		
6.130	1.508 (1)	8.350	1.470 (1)	Ba_{6s}
4.622		6.880		
0.000	0.377 (2)	0.000	0.437 (2)	N_{2p}
−0.377		−0.437		
−0.623	5.417 (35)	−0.742	5.756 (35)	Ba_{4d} N_{2p}
−6.040		−6.498		Si_{3p} O_{2p}
−6.342	0.860 (2)	−6.803	0.863 (2)	N_{2p}
−7.202		−7.666		Si_{3s} O_{2p}
−7.363	1.231 (3)	−7.833	1.280 (3)	Si_{3s}
−8.594		−9.112		
−9.798	0.479 (9)	−10.303	0.523 (9)	Ba_{5p}
−10.277		−10.826		
−14.285	0.302 (2)	−14.402	0.296 (2)	N_{2s}
−14.587		−14.698		
−16.437	0.382 (6)	−16.680	0.371 (6)	O_{2p} Si_{3p}
−16.819		−17.051		
−17.935	1.589 (6)	−18.079	1.514 (6)	O_{2s} Si_{3s}
−19.524		−19.593		
−24.656	0.270 (3)	−23.610	0.426 (3)	Ba_{5s}
−24.926		−24.036		
−80.508	0.040 (5)			Ba_{4d}
−80.548				
−80.821	0.011 (10)			Ba_{4d}
−80.832				
		$Ba_3Si_6O_9N_4$		
5.271	0.890 (1)	7.421	0.970 (1)	Ba_{6s}
4.381		6.451		
0.000	0.352 (4)	0.000	1.053 (4)	N_{2p}
−0.352		−1.053		
−0.435	6.504 (32)	−1.171	5.601 (32)	N_{2p} O_{2p}
−6.939		−6.772		Si_{3p}
−7.367	0.984 (3)	−7.229	1.078 (3)	N_{2p} O_{2p}
−8.351		−8.307		Si_{3s}
−10.051	0.128 (3)	−9.985	0.175 (3)	Ba_{5p}
−10.179		−10.160		
−10.282	0.263 (6)	−10.206	0.324 (6)	Ba_{5p}
−10.530		−10.545		
−13.934	1.172 (4)	−13.920	1.171 (4)	N_{12s} Si_{3p}
−15.106		−15.091		
−16.892	0.411 (6)	−16.878	0.410 (6)	O_{2s} Si_{3s}
−17.303		−17.288		
−18.909	0.391 (3)	−18.892	0.392 (3)	O_{2s} Si_{3s}
−19.300		−19.285		
−24.894	0.274 (3)	−24.879	0.274 (3)	Ba_{5s}
−25.168		−25.153		
−80.716	0.025 (5)			Ba_{4d}
−80.741				
−80.976	0.027 (10)			Ba_{4d}
−81.003				
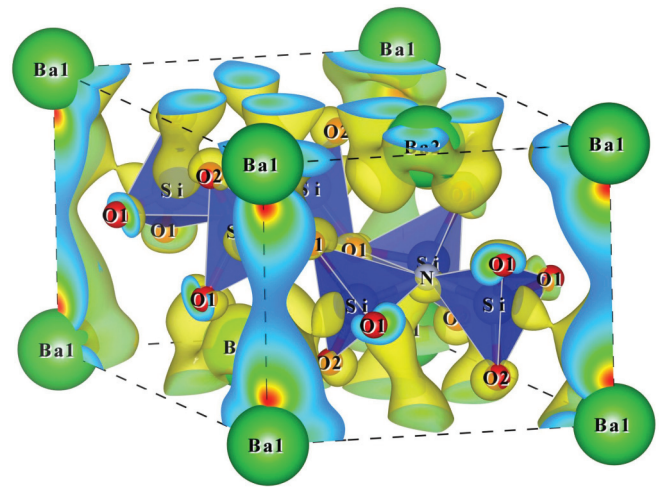
(a) $Ba_3Si_6O_{12}N_2$
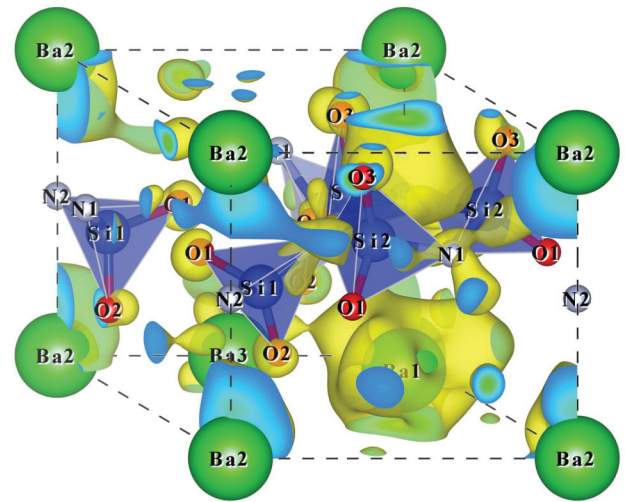
(b) $Ba_3Si_6O_9N_4$

FIG. 7. (Color online) (a) Density of the sum of the 85 to 90th bands of $Ba_3Si_6O_{12}N_2$ at the Γ point that corresponds mainly to the 5d states of barium. (b) Density of the sum of the 81 to 83rd bands of $Ba_3Si_6O_9N_4$ at the Γ point that corresponds mainly to the 5d states of barium. Both isodensity are at 10% of the maximum density of that state.

In order to understand the hybridization, the probability density for wave functions in the zone of energies corresponding to the peak in the DOS, attributed to the 5d states of barium, are also shown in Fig. 7. For $Ba_3Si_6O_{12}N_2$ one clearly sees a large probability density in the region between the Ba_1 atoms, along the z direction, with also some localized d states around Ba_2. For $Ba_3Si_6O_9N_4$ a large probability density is observed around the Ba_1 atoms, with an additional protrusion along the z axis, downwards [so seen through the upper face of Fig. 7(b)]. This protrusion is similar in shape to the one seen in Fig. 5(b). In this region, there is no atom, but three Si tetrahedra building blocks face it directly, as can be seen in Fig. 1(b). No such structure is present in $Ba_3Si_6O_{12}N_2$, see Fig. 1(a).

On the basis of the electronic structure of the undoped hosts only, one can hardly progress further. Careful analysis of the different thermal quenching models requires a complex

analysis including the phononic behavior of the host as done by Mikami.[37,38] The vibrational analysis performed there indicates no significant difference between the two hosts suggesting that the difference in thermal quenching may be explained by the autoionization model rather than the traditional configurational coordinate diagram. The nephelauxetic effect of the 5d europium state in the phosphors should therefore be investigated, but an analysis of the doped compounds will be left for future study as it is beyond the scope of this investigation.

E. Absorption spectra at the RPA level

The last analysis made on the two materials is the computation of the macroscopic dielectric function in the independent particle sum over states approximation (RPA), whose imaginary part is directly linked to the electromagnetic (optical and UV) absorption spectrum. Since both materials have a hexagonal lattice structure, the only two nontrivial components of the dielectric function, probed by the electric field polarization, are $\varepsilon_{xx} = \varepsilon_{yy}$ and ε_{zz}. Both components are compared for the two materials in Fig. 8.

(a) Absorption spectra in the $xx = yy$ direction.

(b) Absorption spectra in the zz direction.
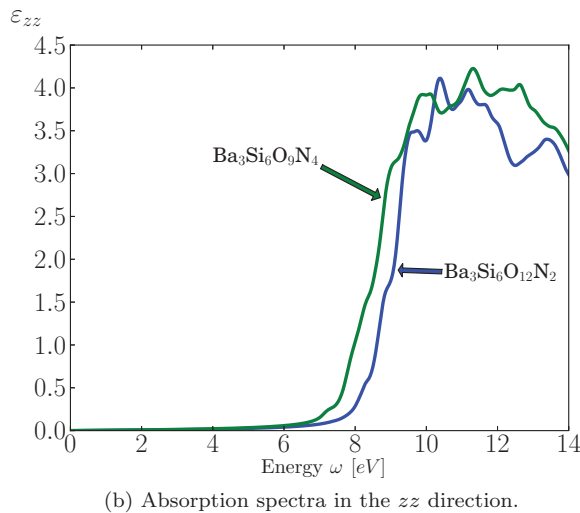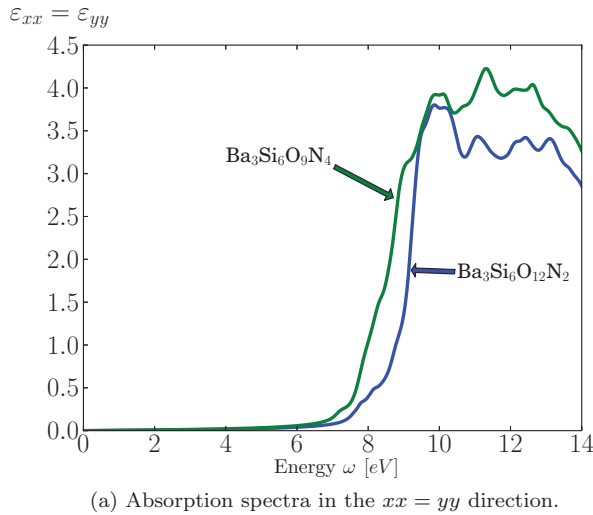
FIG. 8. (Color online) Comparison of the $Ba_3Si_6O_{12}N_2$ and $Ba_3Si_6O_9N_4$ electromagnetic absorption spectra at the RPA level for electric field polarization in the two nontrivial directions.

As anticipated from the G_0W_0 band structure, the onset of absorption occurs at a lower energy in the $Ba_3Si_6O_9N_4$ case. In the quasiplateau region, where the imaginary part of the dielectric function is between 3.0 and 4.5 for both materials and in both directions, we observe a smaller average value for $Ba_3Si_6O_{12}N_2$, although for selected energies, the value observed for $Ba_3Si_6O_{12}N_2$ can be bigger than the one for $Ba_3Si_6O_9N_4$.

The real part of the macroscopic dielectric function at zero electronic frequencies gives a value of 2.38 and 2.80 for $\varepsilon_{xx}^\infty = \varepsilon_{yy}^\infty$ in $Ba_3Si_6O_{12}N_2$ and $Ba_3Si_6O_9N_4$, respectively. The ε_{zz}^∞ component has a value of 2.41 and 2.74 for $Ba_3Si_6O_{12}N_2$ and $Ba_3Si_6O_9N_4$, respectively. These results are made at the RPA level without local field effect. The inclusion of local field effects at the density functional perturbation level (the Hartree and exchange-correlation kernels are included, calculations are done at the GGA level), with the computational parameters detailed in Mikami and Kijima[39] gives 3.10 and 3.30 for $\varepsilon_{xx}^\infty = \varepsilon_{yy}^\infty$ in $Ba_3Si_6O_{12}N_2$ and $Ba_3Si_6O_9N_4$, respectively, and 3.07 and 3.21 for ε_{zz}^∞ in $Ba_3Si_6O_{12}N_2$ and $Ba_3Si_6O_9N_4$, respectively. The anisotropy of these materials, although non-negligible, is thus quite weak, as was already reported in the case of the effective masses.

Some excitonic effects are anticipated (but are outside the scope of this study). We can hypothesize Frenkel excitons will be observed, in view of the relatively low dielectric constants. Indeed a low value for the dielectric constant means a weak screening and, as a result, a tightly bound exciton. Based on this fact, we can deduce that the $Ba_3Si_6O_{12}N_2$ would have a somewhat more strongly bound exciton than $Ba_3Si_6O_9N_4$. The difference between quasiparticle energy gaps, previously shown to be on the order of 0.43 eV, might thus be increased when considering optical energy gaps (although the optical gaps will be smaller than the electronic gaps).

IV. CONCLUSION

The temperature-dependent luminescent properties of $Ba_3Si_6O_{12}N_2$:Eu^{2+} and $Ba_3Si_6O_9N_4$:Eu^{2+} are quite different, despite similar crystallographic structures. In order to understand whether small details, related to the coordination of the Eu ions in the two hosts, are at the heart of the different behavior, we have performed an in-depth analysis of the electronic structure of $Ba_3Si_6O_{12}N_2$ and $Ba_3Si_6O_9N_4$.

The determination of the indirect electronic band gaps of $Ba_3Si_6O_{12}N_2$ with state of the art G_0W_0 techniques, not subject to the well-known DFT band gap problem, gives an electronic band gap of 6.88 eV. This agrees with the experimental results obtained by Braun *et al.*[8] of 7.05 ± 0.25 eV. Such a technique could be used for other phosphors, because it is not straightforward to experimentally evaluate band gaps of powdered phosphor samples, often with Ce or Eu luminescent centers and (possible) unintentional impurities/defects.

Moreover, the difference in the quasiparticle band gap between $Ba_3Si_6O_{12}N_2$ and $Ba_3Si_6O_9N_4$ as calculated with G_0W_0 correction is of 0.43 eV in agreement with the phenomenological interpretation of the quenching mechanisms according to the Dorenbos' scheme (autoionization). The fact that the 5d states of barium are located closer to the conduction band minimum in the $Ba_3Si_6O_9N_4$ compounds

also strengthens that argument. We also have computed the macroscopic dielectric function in the sum over state approximation for both materials. In addition to the straight quasiparticle band structure study, we have also analyzed in detail the characteristics of (i) the valence band edge, directly linked to the nitrogen nonbonding states, two for $Ba_3Si_6O_{12}N_2$ and four for $Ba_3Si_6O_9N_4$, explaining in part the reduction of the band gap in the latter material, (ii) the conduction band edge, similarly dispersive for both materials, although the associated spatial distribution exhibits striking differences, (iii) the nature of the main peak in the DOS of the conduction band, mainly made of Ba_{5d} states, however hybridizing differently in both materials, (iv) the chemical shift at the different barium atomic sites, showing that the large lowering of the energy of the Ba_{5d} peak in $Ba_3Si_6O_9N_4$ with respect to $Ba_3Si_6O_{12}N_2$ is also present for the barium core states, albeit strongly reduced, and (v) the absorption spectrum in the visible-UV range and dielectric constant, showing again strong similarities in both materials, except for the 0.43 eV energy band gap difference.

The present study highlights that the contribution of the valence band modification cannot be neglected in the reduction of the band gap of $Ba_3Si_6O_9N_4$ with respect to $Ba_3Si_6O_{12}N_2$. Actually, the modification of the energy difference between the luminescent level (an excited state) and the conduction band cannot be determined in the present scheme. Thus our accurate band calculation of the host material may not be conclusive in that autoionization is indeed the explanation of the different thermal quenching behavior. The analysis of europium-doped models, also based on many-body perturbation theory, is needed to provide the definite answer to this puzzling behavior. Such an investigation is however very challenging, from the computational point of view, and is left for future study.

---

[*]Bruno Bertrand and Samuel Poncé contributed equally to this work; samuel.ponce@uclouvain.be

[1]M. Nazarov and D. Y. Noh, *New Generation of Europium and Terbium Activated Phosphors* (Pan Stanford, Boca Raton, Florida, 2011).

[2]W. M. Yen, S. Shionoya, and H. Yamamoto, *Phosphor Handbook: Second Edition* (CRC Press, Padstow, Cornwall, 2007).

[3]K. Uheda, S. Shimooka, M. Mikami, H. Imura, and N. Kijima, in *14th International Display Workshop* (Curran Associates, Inc., Red Hook, New York, 2007), p. 899.

[4]M. Mikami, S. Shimooka, K. Uheda, H. Imura, and N. Kijima, Key Eng. Mater. **403**, 11 (2009).

[5]H.-G. Kim, E.-H. Kang, B.-H. Kim, and S.-H. Hong, Opt. Mater. **35**, 1279 (2013).

[6]F. Stadler and W. Schnick, Z. Anorg. Allg. Chem. **632**, 949 (2006).

[7]R. Zhang, M. Numata, T. Maeda, Y. Akazawa, K.-I. Murai, and T. Moriga, Int. J. Mod. Phys. B **24**, 3221 (2010).

[8]C. Braun, M. Seibald, S. Börger, O. Oeckler, T. Boyko, A. Moewes, G. Miehe, A. Tücks, and W. Schnick, Chem. Eur. J. **16**, 9646 (2010).

[9]J. Tang, J. Chen, L. Hao, X. Xu, W. Xie, and Q. Li, J. Lumin. **131**, 1101 (2011).

[10]D. G. Porob, S. Kishore Manepallib, N. P. Kumarb, and A. Setlur, ECS Trans. **33**, 101 (2011).

[11]Y. H. Song, T. Y. Choi, K. Senthil, T. Masaki, and D. H. Yoon, Mater. Lett. **65**, 3399 (2011).

[12]E.-H. Kang, S.-W. Choi, and S.-H. Hong, ECS J. Solid State Sci. Technol. **1**, R11 (2012).

[13]P. Dorenbos, J. Phys.: Condens. Matter **17**, 8103 (2005).

[14] The accuracy of band gap evaluation is necessary for the discussion on thermal quenching, by considering Dorenbos' empirical formula: $\Delta E = T_{0.5}/680$ eV, where $T_{0.5}$ is the quenching temperature at which the emission intensity has dropped to 50% of the low temperature value and ΔE is the energy barrier.[13]

[15]R. M. Martin, *Electronic Structure. Basic Theory and Practical Methods* (Cambridge University Press, Cambridge, 2004).

[16]J. P. Perdew, K. Burke, and M. Ernzerhof, Phys. Rev. Lett. **77**, 3865 (1996).

[17]D. Waroquiers, A. Lherbier, A. Miglio, M. Stankovski, S. Poncé, M. J. T. Oliveira, M. Giantomassi, G.-M. Rignanese, and X. Gonze, Phys. Rev. B **87**, 075121 (2013).

[18]W. G. Aulbur, L. Jönsson, and J. W. Wilkins, *Solid State Physics*, Vol. 54 (Academic Press, Waltham, Massachusetts, 1999), pp. 1–218.

[19]M. van Schilfgaarde, T. Kotani, and S. Faleev, Phys. Rev. Lett. **96**, 226402 (2006).

[20]S. Curtarolo, G. Hart, M. B. Nardelli, N. Mingo, S. Sanvito, and O. Levy, Nat. Mater. **12**, 191 (2013).

[21]P. E. Blöchl, Phys. Rev. B **50**, 17953 (1994).

[22]J. P. Perdew, K. Burke, and M. Ernzerhof, Phys. Rev. Lett. **77**, 3865 (1996).

[23]N. Holzwarth, A. Tackett, and G. Matthews, Comput. Phys. Commun. **135**, 329 (2001).

[24]http://www.abinit.org/downloads/PAW2.

[25]W. H. Press, B. P. Flannery, S. A. Teukolsky, and W. T. Vetterling, *Numerical Recipes (Fortran)* (Cambridge University Press, Cambridge, 1989).

[26]M. Giantomassi, M. Stankovski, R. Shaltaf, M. Grüning, F. Bruneval, P. Rinke, and G.-M. Rignanese, Phys. Status Solidi B **248**, 275 (2011).

[27]H. J. Monkhorst and J. D. Pack, Phys. Rev. B **13**, 5188 (1976).

[28] R. Shaltaf, T. Rangel, M. Grüning, X. Gonze, G.-M. Rignanese, and D. R. Hamann, Phys. Rev. B **79**, 195101 (2009).

[29] F. Bruneval and X. Gonze, Phys. Rev. B **78**, 085125 (2008).

[30] R. W. Godby and R. J. Needs, Phys. Rev. Lett. **62**, 1169 (1989).

[31] S. Lebègue, B. Arnaud, M. Alouani, and P. E. Bloechl, Phys. Rev. B **67**, 155208 (2003).

[32] D. Bohm and D. Pines, Phys. Rev. **92**, 609 (1953).

[33] X. Gonze, B. Amadon, P.-M. Anglade, J.-M. Beuken, F. Bottin, P. Boulanger, F. Bruneval, D. Caliste, R. Caracas, M. Côté, T. Deutsch, L. Genovese, P. Ghosez, M. Giantomassi, S. Goedecker, D. Hamann, P. Hermet, F. Jollet, G. Jomard, S. Leroux, M. Mancini, S. Mazevet, M. Oliveira, G. Onida, Y. Pouillon, T. Rangel, G.-M. Rignanese, D. Sangalli, R. Shaltaf, M. Torrent, M. Verstraete, G. Zerah, and J. Zwanziger, Comput. Phys. Commun. **180**, 2582 (2009).

[34] K. Momma and F. Izumi, J. Appl. Crystallogr. **44**, 1272 (2011).

[35] P. Dorenbos, J. Phys.: Condens. Matter **15**, 2645 (2003).

[36] M. Oshikiri, F. Aryasetiawan, Y. Imanaka, and G. Kido, Phys. Rev. B **66**, 125204 (2002).

[37] M. Mikami, Opt. Mater., doi: 10.1016/j.optmat.2012.11.014.

[38] M. Mikami, ECS J. Solid State Sci. Technol. **2**, R3048 (2013).

[39] M. Mikami and N. Kijima, Opt. Mater. **33**, 145 (2010).